Stony Brook University

Effects of residual solvent molecules facilitating the infiltration synthesis of ZnO in a non-reactive polymer

A Thesis Presented

by

Xinyi Ye

to

The Graduate School

in Partial Fulfillment of the

Requirements

for the Degree of

Master of Science

in

Materials Science and Engineering

Stony Brook University

May 2017

Stony Brook University

The Graduate School

Xinyi Ye

We, the thesis committee for the above candidate for the

Master of Science degree, hereby recommend

acceptance of this thesis.

Dr. Chang-Yong Nam
Adjunct Professor
Center for Functional Nanomaterials
Brookhaven National Laboratory

Dr. T. Venkatesh
Associate Professor, Graduate Program Director
Materials Science and Chemical Engineering
Stony Brook University

Dr. Tae Jin Kim
Assistant Professor
Materials Science and Chemical Engineering
Stony Brook University

This thesis is accepted by the Graduate School

Charles Taber
Dean of the Graduate School

Abstract of the Thesis

Effects of residual solvent molecules facilitating the infiltration synthesis of ZnO in a non-reactive polymer

by

Xinyi Ye

Master of Science

in

Materials Science and Engineering

Stony Brook University

2017

Infiltration synthesis, the atomic-layer-deposition-based organic-inorganic material hybridization technique that enables unique hybrid composites with improved material properties and inorganic nanostructures replicated from polymer templates, is shown to be driven by the binding reaction between reactive chemical groups of polymers and perfusing vapor-phase material precursors. Here, we discover that residual solvent molecules from polymer processing can react with infiltrating material precursors enabling the infiltration synthesis of metal oxides in a non-reactive polymer. The systematic study, combining in-situ quartz crystal microgravimetry, polarization-modulated infrared reflection-absorption spectroscopy, X-ray photoelectron spectroscopy, and transmission electron microscopy, shows that the ZnO infiltration synthesis in nominally non-reactive SU-8 polymer is mediated by residual processing solvent cyclopentanone, a cyclic ketone whose Lewis-basic terminal carbonyl group can react with the infiltrating Lewis-acidic Zn precursor diethylzinc (DEZ). In addition, we find favorable roles of residual epoxy rings in the SU-8 film in further assisting the infiltration synthesis of ZnO. The discovered rationale not only improves the understanding of infiltration synthesis mechanism but also potentially expands its application to more diverse polymer systems for the generation of unique functional organic-inorganic hybrids and inorganic nanostructures.

Table of Contents

List of Figures/Tables/Illustrations

List of Abbreviations

ALD	Atomic layer deposition
SIS	Sequential infiltration synthesis
CP	Cyclopentanon
GBL	γ-butyrolactone
TMA	Trimethylaluminum
DEZ	Diethylzinc
PAG	Photo-acid generators
PMMA	Poly(methyl methacrylate)
P3HT	Poly(3-hexylthiophene)
QCM	Quartz crystal microgravimetry
PM-IRRAS	Polarization-modulated infrared reflection-absorption spectroscopy
TEM	Transmission electron microscope
XPS	X-ray photoelectron spectroscopy

Acknowledgments

Foremost, I would like to express my sincere gratitude to my advisor Prof. Chang-Yong Nam for the continuous support of my master study and research, for his patience, motivation, enthusiasm and encouragement. His guidance helped me in all the time of research and writing of the thesis and paper.

Besides my advisor, I would like to thank other scientists at CFN: Dr. Kim Kisslinger for preparing TEM samples and imaging, Dr. Mingzhao Liu for verifying the chemical reaction routes, Dr. J. Anibal Boscoboinik for insightful comments on XPS and IR data.

My sincere thank also goes to Dr. John Kestell, for giving me the opportunity to learn PM-IRRAS and to apply this great technique to my research.

I am grateful for the facilities and resources at the Center for Functional Nanomaterials (CFN), Brookhaven National Laboratory (BNL), which is supported by the U.S. Department of Energy.

Chapter

1. INTRODUCTION

Infiltration synthesis is a type of material hybridization process derived from atomic layer deposition (ALD), where vapor-phase material precursors infiltrate into a polymer matrix, enabling the generation of organic-inorganic hybrids as well as inorganic replicas of starting polymer templates when the polymer is selectively removed.[1–4] Depending on the specific protocol governing the precursor exposure sequences, the multi-pulse infiltration,[5] sequential infiltration synthesis,[6–9] and sequential vapor infiltration,[10] have been developed over the past few years, and they have been proven useful for enhancing various properties of polymers, such as mechanical strength,[11,12] photoluminescence,[13,14] photocatalytic activity,[15] oil absorption ability,[16] and triboelectric properties.[6,17] The nanoparticles deposited by infiltration synthesis also had a superior thermal stability and spatial separation that were useful for catalytic applications.[18] Also demonstrated was the application of the technique for creating inorganic nanopatterns derived from self-assembled block copolymer thin films[2,8,9] with novel properties such as enhanced optical anti-reflectivity,[19] mesoporous metal oxide monolith converted from polymer microfibers,[10] and inorganic nanopatterns converted from lithographically patterned polymer templates [7,20] such as the electrically active ZnO nanowire arrays that could be integrated into field-effect transistors as we reported recently.[21]

For applying the infiltration synthesis within a given polymer system, the binding reaction between Lewis-acidic vapor-phase organometal precursors and Lewis-basic functional groups in the polymer was shown to be critical,[15,22,23] with the binding reaction rate and kinetics being affected by temperature, choice of precursors, available functional groups in polymers, and infiltration protocols governing the precursor exposure/purge durations and schemes.[14,15,22–25] So far, most reported studies on the infiltration synthesis mechanism have been based on the polymer systems with known functional groups that could react with material precursors, specifically trimethylaluminum (TMA) for the infiltration synthesis of Al_2O_3.[26–29] For instance, Biswas et al. reported that TMA initially formed a weakly-bound complex with pendent C=O and C-O-R functional groups in poly(methyl methacrylate) (PMMA) during the sequential infiltration synthesis process.[22,29] Other groups also demonstrated that TMA reacted with certain nucleophilic carbonyl groups in polyester fibers either on the surface or within the bulk.[12,14,27,30] These studies overall suggest the requirement of specific reactive functional groups in the polymer for the successful infiltration synthesis.

While the interaction of TMA with polymers has been extensively studied for understanding the infiltration synthesis of Al_2O_3, there have been few reports that investigated the infiltration synthesis mechanism of other materials, such as ZnO, a more electrically functional metal oxide that is typically generated from diethylzinc (DEZ) used as a material precursor. Most reported ZnO infiltration synthesis required the pre-infiltration synthesis of Al_2O_3 (i.e., "priming") that acted as nucleation sites, except one recent study that suggested that the polymer crystallinity could facilitate the ZnO infiltration into a non-reactive polymer, poly(3-hexylthiophene) (P3HT).[31] However, such an effect of polymer crystallinity cannot be generally applied to non-crystalline polymers, such as SU-8, a well-known epoxy-based negative-tone (i.e., cross-linkable) polymer photoresist, widely used in microelectronics,[32] microfluidics,[33] waveguides,[34] and chemical sensors.[35] Recently, we reported the infiltration synthesis of ZnO, along with Al_2O_3 and TiO_2, in patterned (cross-linked) SU-8 templates without Al_2O_3 priming process, demonstrating various, arbitrarily designed metal oxide nanostructures with high aspect ratios as well as controlled geometries and spatial registrations.[21,36] Despite the successful application of SU-8 as polymer templates for the infiltration synthesis, one unusual aspect of SU-8 is that unlike PMMA and polyester, the nominal chemical structure of cross-linked SU-8 primarily consists of C-O-C (ether) type backbone bonding[37,38], which is not expected to readily bind with the vapor precursors of the demonstrated infiltration-synthesized metal oxides, compared with other more reactive functional groups such as the pendent C=O and C-O-R groups in PMMA.[21,28]

In this work, we investigate the infiltration synthesis mechanism of ZnO in the cross-linked SU-8 thin film to understand the nature of the chemical interaction between the ZnO material precursor and the nominally non-interacting SU-8. We discover that residual solvent molecules from the polymer processing mediate the infiltration synthesis of ZnO in the non-reactive SU-8 by reacting with perfusing Zn precursor. We infiltration-synthesized ZnO using DEZ and water as material precursors in the cross-linked thin-film SU-8. The in-situ quartz crystal microgravimetry (QCM) measurement during the infiltration synthesis and the post-synthesis cross-sectional transmission electron microscopy (TEM) indeed showed the mass gain and structural characteristics consistent with the material infiltration *into* the polymer although the SU-8 nominally had no known strong reactive chemical moieties such as carbonyl groups. Surprisingly, the polarization-modulated infrared reflection-absorption spectroscopy (PM-IRRAS) identified the existence of carbonyl (C=O) groups in the starting SU-8 film as well as their consumption after the infiltration synthesis. We confirmed that the C=O groups were originating from the cyclic ketone SU-8 processing solvent, cyclopentanone (CP), by monitoring

the varying C=O contents with respect to the film thermal baking condition. The identified solvent effect was further confirmed by testing a different (cyclic ester) processing solvent with C=O group, γ-butyrolactone (GBL), which permitted a different degree of ZnO infiltration synthesis compared with CP as supported by the QCM and X-ray photoelectron spectroscopy (XPS) data. The in-depth analysis of PM-IRRAS data revealed potential reaction mechanisms between the perfusing DEZ and the SU-8 film, involving the interaction of DEZ with residual solvent molecules as well as uncross-linked epoxy rings and polymer ether backbones, potentially assisted by the short-range anisotropic alignment of polymer chains within the film. This newly discovered role of solvent molecules enabling the infiltration synthesis in a nominally non-reactive polymer not only suggests a new pathway for the infiltration synthesis process but also potentially expands the applicability of infiltration synthesis to more diverse polymer systems for the generation of unique functional organic-organic hybrids and metal oxide nanostructures.

2. EXPERIMENTAL DETAILS

Chemicals and materials

We used commercially available SU-8 solutions (MicroChem) and organic solvents (Sigma-Aldrich), including CP and GBL, as received. Two different series of SU-8 photoresist solutions were used in the experiments, SU-8 2002 diluted in CP and SU-8 25 in GBL. Bare Si substrates were used for preparing TEM and XPS samples, while Si substrates with 40 nm-thick Au coating were used for PM-IRRAS (Au was coated by a sputter coater (Cressington 208HR)). The diluted SU-8 solutions of varying concentrations were spin-cast on the substrates at 2000 rpm, followed by ambient pre-cross-linking baking for 1 min at 65 $^{\circ}$C and additional 3 min at 95 $^{\circ}$C on a hot plate (i.e., soft bake). The samples were then exposed to ultraviolet (UV) light for 5 min under nitrogen using a UV light chamber equipped with a low-pressure mercury lamp (American Ultraviolet Co.), followed by the post-exposure bake for 2 min at 95 $^{\circ}$C in ambient air. The film thickness was measured by an interferometer (Filmetrics). The thickness of SU-8 thin films was varied from 40 nm, 70 nm, 100 nm, and to 135 nm for PM-IRRAS measurement. For TEM and XPS characterization, thicker SU-8 2002 films (< 200 nm) were used.

ZnO infiltration synthesis and in-situ mass gain measurement

We infiltration-synthesized ZnO in the spin-coated SU-8 films at 85 °C using a commercial ALD system (Cambridge Nanotech Savannah S100). DEZ (Aldrich) was used as an organometallic precursor of ZnO. Typically, one ZnO infiltration synthesis cycle consists of the following steps (Scheme 1 (a)): The DEZ vapor was first introduced into the reactor, and the reactor was immediately isolated to allow DEZ to diffuse into the polymer matrix for 300 sec (chamber pressure ~1.6 Torr). The reactor was then pumped/purged with 100 sccm N_2 flow for 60 sec (for removing the surface-adsorbed excess DEZ that can form thick ZnO layer and block the precursor infiltration during the following ZnO infiltration synthesis cycles), which was followed by the water vapor exposure to the polymer templates for 300 sec (pressure ~10 Torr) and pumping/purging in 100 sccm N_2 for 300 sec for removing excess water molecules from exposed surfaces (representative mass gain variation characteristics during the exposure and purging steps are given in Figure. S1). The ZnO infiltration synthesis cycle was repeated for multiple times as desired. For the in-situ mass gain measurement during the infiltration synthesis, we used a QCM system installed in the ALD reactor. A thick SU-8 film (>1 μm) processed with the desired solvent was spin-cast onto a quartz crystal (Philips Technologies, Au-plated, 6 MHz resonant frequency, 14 mm diameter, AT-cut). The QCM crystal was then mounted onto the sensor head (Colnatec, Inc.) installed in the reactor. The temperature of the integrated heater on the QCM sensor head was set identical to the reactor temperature. Before the infiltration synthesis process, we let the sensor temperature equilibrate with the chamber temperature and stabilize for 1-2 hr to minimize the QCM background signal drift originating from the temperature variation. The change in the resonance frequency of the SU-8-coated quartz crystal was recorded during the process and converted into a mass gain value by the Sauerbrey equation,[39] using the sensitivity factor of 81.2 Hz $\mu g^{-1} cm^2$ for the AT-cut crystal used in our experiments.

Structural and chemical characterization

The internal structures of the SU-8 thin films, before and after 2 or 10 cycles of ZnO infiltration synthesis, were examined by cross-sectional high-resolution TEM (JEOL 2100F, 200 kV). The cross-sectional TEM samples were prepared by the in-situ lift-out technique in a focused ion beam (FIB) system (FEI Helios) using carbon and top Au protective layers applied on top of the samples. Energy dispersive X-ray spectroscopy (EDXS) was also carried out to identify the infiltration-synthesized ZnO within the polymer matrix. The change of chemical bonding

characteristics on the SU-8 surface before and after the ZnO infiltration synthesis was studied by XPS. Only one infiltration synthesis cycle was applied to ensure the absence of dense ZnO top layer that tended to form under the increasing number of synthesis cycle. We used a home-built XPS system equipped with a PHOIBOS hemispherical electron energy analyzer (SPECS) and Mg K_α X-ray source (1.254 keV, SPECS). The XPS study was complemented by the PM-IRRAS measurement, an IR spectroscopy technique sensitive for measuring the chemical structure and molecular orientation of molecular monolayers and ultrathin films coated onto metal surfaces.[40] At a high grazing incidence angle, the absorption of p-polarized IR light on a metal surface is largely enhanced while that of s-polarized light is virtually zero for the species close to the metal surface.[40–42] This can be utilized for obtaining the chemical bonding characteristics as well as the chain orientation and conformation at the *bottom* of SU-8 thin films before and after the infiltration synthesis. The measurements were performed in a home-built PM-IRRAS system described in detail in our earlier study.[43] The system was equipped with a Bruker Vertex 80v spectrometer, and the IR beam was p-polarized with a ZnSe grid polarizer and reflected from the surface plane at an 8-degree angle. All spectra were recorded with a liquid-nitrogen-cooled HgCdTe detector (InfraRed Associates).

3. RESULTS AND DISCUSSION

3.1. Mass gain and structural characteristics of ZnO infiltration synthesis in SU-8

The in-situ QCM measurement confirmed the mass gain characteristics of ZnO infiltration synthesis in SU-8 distinguished from those expected in a normal ALD ZnO growth on the surface. The mass gain of a typical SU-8 film (processed with CP as a solvent) was measured during the first 20 cycles of ZnO infiltration synthesis (Figure 1 (a)). The first cycle displayed a relatively large mass uptake (~2.0 μg/cm^2) while the following cycles showed a lower, constant mass uptake of 0.68 μg/cm^2 per cycle, which corresponds to an equivalent ZnO thickness of ~10.2 Å per cycle (assuming the density of ZnO is 5.61 g/cm^3), a value nearly 15 times larger than a typical growth rate of ZnO during the normal ALD process (~0.7 Å/cycle at 85 °C).[44] These data clearly indicate a bulk growth mode, not controlled by the self-limited surface reaction but rather mediated by the precursor's penetration into and subsequent hybridization with the polymer matrix, during the infiltration synthesis. The mass gain per cycle during the first infiltration synthesis cycle is nearly three times larger than that of the subsequently following cycles, which we expect to be related to the initial consumption of the polymer free

volume during the first synthesis cycle. The internal structure of the ZnO-infiltrated SU-8 films examined by the cross-sectional TEM was consistent with the bulk growth mode of ZnO infiltration synthesis as observed in the in-situ mass gain measurement: The bright-field TEM image in Figure 1 (b) reveals that the ZnO infiltration synthesis already occurred down to ~50 nm below the surface after only two cycles of ZnO infiltration synthesis. The dark contrast in the upper portion of the SU-8 film, originating from the atomic number (Z) contrast, is where most ZnO infiltration synthesis has occurred, and the corresponding EDS line scan (Zn K_α) confirmed the ZnO infiltration profile (Figure 1 (c)). We found that the ZnO infiltration depth was not really changing with increasing number of synthesis cycles as shown in the cross-sectional TEM micrograph obtained from the 10-cycle-infiltrated SU-8 (Figure S2). The increased Z-contrast in the 10-cycle condition (Figure S2) compared with the 2-cycle sample (Figure 1(b)) also indicates a continued ZnO infiltration as the number of infiltration synthesis cycles increased, showing that the large mass gain during the first few ZnO infiltration cycles did not fully saturate the free volume available in the polymer matrix, allowing the precursor infiltration into the polymer matrix during the following infiltration synthesis cycles.

Overall, the observed mass gain trend and internal structure agree with what has been observed in other infiltration studies,[3,30] confirming that the dominant ZnO deposition mode in our experiments was the infiltration synthesis despite the nominal absence of reactive terminal carbonyl groups in the cross-linked SU-8. Typically, the SU-8 solution consists of epoxy-based monomers and a minor quantity (typically, 1-5 wt.% according to the manufacturer specification) of photo-acid generators (PAG) in a certain organic solvent, such as CP. Scheme 1 (b) shows the nominal chemical structures of SU-8 monomer, CP, and PAG molecules we used. The PAG is an onium salt, triarylsulfonium hexafluoroantimonate ($(Ar)_3S^+SbF_6^-$), which decomposes to acidic $H^+SbF_6^-$ upon UV exposure and catalyzes the cross-linking reaction of the monomers (i.e., reaction among epoxy rings) in the SU-8 film during the post-exposure thermal baking (Scheme 1 (c)).[45] The resultant cross-linked SU-8 structure primarily contains -C-O-C- type ether bonds along the polymer network,[38] which are expected to be stable and do not form strong chemical bonds with organometallic precursors. This hints a plausibility that the observed ZnO infiltration synthesis in the cross-linked SU-8 is not relying on the direct reaction between the organometallic precursor and the polymer matrix itself as observed in the typical infiltration synthesis studies performed on more reactive polymers.[22]

3.2. Effects of ZnO infiltration synthesis on the chemical bonding characteristics of SU-8

To further investigate potential factors that could enable the ZnO infiltration synthesis in the non-reactive cross-linked SU-8, we examined the chemical bonding characteristics of the SU-8 thin film before and after the infiltration synthesis by PM-IRRAS. Figure 2 (a) shows the IR absorption spectrum measured by PM-IRRAS from the typically prepared cross-linked SU-8 thin film (40 nm thick) without ZnO infiltration synthesis (i.e., processed in CP as a solvent; soft-baked, UV-exposed, and post-exposure-baked), where the absorption peaks at 1250 cm^{-1} and 830 cm^{-1} originate from epoxy rings, and the groups of peaks in the 1700-1400 cm^{-1} region correspond to para- and ortho-substituted benzene rings.[35] The detailed assignment of the peaks to corresponding vibration modes can be found in Table 1, with each peak labeled in Figure 2 (b). Along with the peaks at 1250 and 830 cm^{-1}, the peak at 915 cm^{-1} also corresponds to the bending of CH_2 group on the epoxy ring, suggesting an incomplete cross-linking (i.e., incomplete consumption of epoxy rings) of the SU-8 film after the typical cross-linking procedures we applied. This is not unusual as the full cross-linking of SU-8 is known to require a post-exposure bake over 20 min,[37] and the peak at 915 cm^{-1} is usually used to evaluate the degree of cross-linking for this resin.[35,45]

A more surprising feature in the IR absorption spectrum is the presence of the absorption peak at 1735 cm^{-1}, which is typically attributed to a C=O carbonyl group (i.e., a reactive functional group that can enable the infiltration synthesis), which is not expected to exist in the nominal SU-8 structure. The only C=O-group-containing chemical entity used during the SU-8 sample preparation was the solvent, CP, and we confirm that the carbonyl peak was indeed originating from the residual CP molecules in the cross-linked SU-8 film by varying the SU-8 film baking procedure and thus controlling the amount of residual CP in the SU-8: During the preparation of cross-linked SU-8 films, the soft bake step is generally performed for removing processing solvent from the film before cross-linking. When we omitted this step, the intensity of carbonyl absorption peak significantly increased (Figure 2 (a)), clearly showing that the observed carbonyl feature was directly associated with the residual CP in the SU-8 film. A similar IR absorption peak was previously observed in the SU-8 processing study wherein CP was used as a solvent,[38] and overall, this indicates that the solvent molecules will be present in the SU-8 film during the following infiltration synthesis, without being evaporated out of the film. It is interesting to note that even after an extended thermal baking (tested for 24 hr, under ~200 mTorr vacuum, at 150 °C), the solvent molecules appeared to be still present in the SU-8 film; in fact, the C=O absorption peak intensity after the vacuum annealing for 24 hr was nearly the same

as what was observed after the standard soft bake performed for much shorter time under an ambient air (Figure S3). Potentially, some portion of this C=O peak intensity might be from the carbonyl groups formed by the selective rearrangement of residual epoxy rings to ketones,[46] being promoted by Lewis-acidic SbF_5 (originating from PAG), which regardless will be beneficial for the infiltration synthesis.

After we applied the ZnO infiltration synthesis in the cross-linked SU-8, we find that the intensity of the carbonyl absorption peak had decreased, a strong indication that the infiltrating ZnO precursors were reacting with the C=O groups of the residual CP in the SU-8 film during the infiltration synthesis. Figure 2 (c) shows the PM-IRRAS spectra of the cross-linked SU-8 films prepared by the standard procedure (including soft bake), before and after 4 cycles of ZnO infiltration synthesis. The IR absorption intensity of C=O group at 1735 cm^{-1} decreased markedly after the infiltration synthesis with a negligible change in the peak position. This shows the consumption of the C=O groups of the solvent molecules during the ZnO infiltration synthesis, most likely, via the reaction with the infiltrating DEZ. Such a consumption of reactive functional groups in polymers during the infiltration synthesis has been identified for the case of Al_2O_3 infiltration synthesis in PMMA, whose side carbonyl groups acted as nucleation sites within the bulk of the polymer for the reaction with the infiltrating organometallic precursor (TMA) to form -C-O-Al-R bonds after the infiltration synthesis.[3,27] In the present case, the direct observation of Zn-O bonding features in the PM-IRRAS spectra was not available because the Zn-O stretching mode at 433 cm^{-1} was out of the spectral range that our system could cover.[47]

The complementary XPS measurements confirmed the formation of the Zn-O bonding in SU-8 after the ZnO infiltration synthesis, supporting the formation of ZnO in SU-8. Table 2 summarizes the deconvoluted bonding species obtained from the O 1s and C 1s spectral regions. The XPS survey spectra immediately showed the Zn-related peaks after 1 cycle of ZnO infiltration synthesis in SU-8 (Figure 3 (a)). The high-resolution scan over the O 1s region in the control SU-8 without the ZnO infiltration showed a spectrum primarily consisting of -C-O-C- ether (binding energy (B.E.) = 532.9 eV) with a shoulder originating from the oxidized forms of Sb (Sb 3d), the base element for PAG in SU-8 (Figure 3 (b) top). Once subjected to 1 cycle of ZnO infiltration synthesis (Figure 3 (b) bottom), there was a shift in the apparent peak position (indicated by an arrow). The spectrum deconvolution revealed that this was in fact caused by the formation of Zn-OH group, a result of the reaction between the terminal ethyl group of DEZ and water (i.e., $-Zn-C_2H_5 + H_2O \rightarrow -Zn-OH + C_2H_6$), confirming the formation of ZnO. Additionally,

there was a broadening of the shoulder region, stemming from the formation of metallic Sb (Sb $3d_{5/2}$, B.E. = 528 eV) that we suspect to result from the reduction of Sb oxides by DEZ. It is noted that potentially, there exists a Zn-O (O 1s) peak at B.E. = ~530 eV, but this could not be resolved due to its overlap with the pre-existing Sb_2O_3 peak (Sb $3d_{5/2}$). Meanwhile, the comparison of the C 1s region XPS spectra before and after 1 cycle of ZnO infiltration only revealed a minor difference (Figure 3 (c)); a Zn-C (C 1s) peak at B.E. = ~283 eV emerged after the infiltration synthesis, indicating the presence of some unreacted ethyl groups of DEZ (i.e., -Zn-C_2H_5).

We note that a closer examination of the PM-IRRAS spectra obtained after the ZnO infiltration revealed the spectral features that further supported the non-reactive nature of the cross-linked SU-8 network while suggesting a potential assistance of uncross-linked epoxy rings to the ZnO infiltration synthesis (Figure 2 (c)). Specifically, the decrease of solvent carbonyl peak intensity after the ZnO infiltration was accompanied by the increase in ether -O-C-C stretching at 1128 cm^{-1} (originating from the cross-linked SU-8 network) and the decrease in C-O-C stretching of epoxy rings at 1250 cm^{-1} (from uncross-linked epoxy rings). It is noted that ether-containing polymers (e.g., polyethylene oxide (PEO)) and other polymers with methyl ether terminal groups (such as polybutylene terephthalate (PBT) and polylactide (PLA)) have shown the *decrease* of ether stretching intensity after the infiltration synthesis of Al_2O_3, which was ascribed to the reaction between TMA and the ether groups.[27] The observed *increase* of ether -O-C-C stretching after the ZnO infiltration synthesis in our case thus indicates that such a direct reaction between DEZ and the -O-C-C ether groups in the cross-linked SU-8 network was not really occurring. Instead, the increase of -O-C-C ether population is most likely resulting from the decomposition of uncross-linked epoxy rings (i.e., ring opening and cross-linking) in the SU-8 by the infiltration synthesis, which is supported by the observed decrease in epoxy C-O-C stretching intensity at 1250 cm^{-1}. The epoxy ring opening can be initiated by the applied heat during the infiltration synthesis or by the reaction with the infiltrating DEZ, both under the presence of hydroxyl groups (e.g., water). However, the SU-8 film before and after the infiltration synthesis did not feature an observable sign of hydroxyl group in the PM-IRRAS spectra (Figure S4, ~3400 cm^{-1} region for the O-H stretching mode),[48,49] which most likely results from the near full consumption of available hydroxyl groups in the bottom portion of SU-8 film during the first few infiltration synthesis cycles (note that the PM-IRRAS signal exclusively originates from the material near the Au-coated substrate surface). Considering the lower temperature used for the infiltration synthesis (85 °C) compared with the post-UV-

exposure baking temperature (95 °C) designed for the cross-linking of SU-8 under the presence of the acid generated by PAG, the thermally initiated epoxy ring opening is unlikely. Instead, the direct reaction between infiltrating DEZ and uncross-linked epoxy rings in the SU-8 appears to be the most plausible scenario, mediating the retention of infiltrating DEZ within SU-8 and assisting the ZnO infiltration synthesis.

3.3. Effects of a different SU-8 processing solvent

We find that the extent of ZnO infiltration synthesis in SU-8 is dependent on the type of process solvents, further verifying the role of residual solvent molecules affecting the ZnO infiltration synthesis: When we replaced the SU-8 processing solvent from CP (cyclic ketone) to γ-butyrolactone (GBL, cyclic ester), there was a significant decrease (by ~26 %) in the mass gain per ZnO infiltration synthesis cycle, from ~0.68 μg/cm^2 to ~0.50 μg/cm^2 (Figure 4 (a)). The IR absorption measured by PM-IRRAS in the GBL-processed SU-8 exhibited a carbonyl absorption peak at 1735 cm^{-1} before the infiltration synthesis and its reduction in intensity after 4 cycles of ZnO infiltration synthesis (Figure 4 (b), indicated by an arrow), a qualitatively identical trend observed in the CP-processed SU-8. However, one major difference was that the starting carbonyl absorption intensity was much lower (by ~50%, integrated intensity) than that of the CP-processed SU-8 (Figure 4 (b) inset), and this agrees with the decreased mass gain per cycle during the ZnO infiltration synthesis when GBL was used. The carbonyl peak position observed from the GBL-processed SU-8 was found to be nearly identical to that of the CP-processed sample, both of them showing peak shifts compared with the generally known C=O peak positions of the pure solvent molecules (1770 cm^{-1} for GBL and 1747 cm^{-1} for CP),[50,51] which are suspected to be caused by the confinement of the solvent molecules in the polymer matrix and the interaction with the environment.[52] The QCM and IR absorption data overall indicate a smaller concentration of C=O carbonyl groups in the GBL-processed SU-8 compared with the CP-processed one, which appears counter-intuitive considering the higher boiling point (i.e., lower vapor pressure) of GBL (204 °C) than that of CP (131 °C). Given the ambient processing (i.e, the presence of moisture) of SU-8 and the presence of photo-generated acid, we suspect GBL can be potentially decomposed by the acid-catalyzed hydrolysis and converted to more volatile species (1-propanol and CO_2) that are removed from the film during the post-exposure baking procedure.[53] Meanwhile, the XPS spectra obtained from the GBL-processed SU-8 before and after the 4 cycles of ZnO infiltration synthesis were nearly identical to what was observed

from the CP-processed SU-8, confirming the formation of Zn-O bonding (Figure S5 and Table S1). It is interesting to note that the mass gain in the first synthesis cycle was independent of the type of solvent we used and was always larger than that of the subsequent cycles (Figure 4 (a)). This again suggests a large consumption of the polymer free volume, where the reaction of physically trapped DEZ molecules with water is expected to proceed in a random manner similar to the chemical vapor deposition (i.e., uncoordinated), thus making the mass gain during the first synthesis cycle less controlled by the reactivity of residual solvent molecule, but rather more limited by the initially available polymer free volume.

3.4. Potential reaction routes and factors enabling the ZnO infiltration synthesis in SU-8

Reaction between DEZ and carbonyl groups of CP: Considering that DEZ is generally used in the catalytic asymmetric addition to aldehydes or ketones to form alcohols,[54,55] we propose a similar addition reaction mechanism between Lewis-acidic DEZ and the Lewis-basic carbonyl groups in CP (Scheme 2 (a)): The polarity of C=O bond of CP makes it susceptible to ethyl carbanions, byproducts of DEZ decomposition, and may undergo the addition reaction; the nucleophilic oxygen coordinates with Zn atom, and the anionic alkyl group then can react with the electrophilic carbon of the carbonyl group, leading to the ethyl addition and the formation of C-O-Zn- and C-CH_2-CH_3 bonds. The consequences are the consumption of carbonyl groups and the generation of the Zn-O bond, which are consistent with the decrease of carbonyl peak intensity in the PM-IRRAS spectra as well as the observed Zn-O bond formation in the XPS measurement. For other organometallic precursors such as TMA, a similar addition reaction to ketones can be achieved either with or without catalysts,[56] and it has been reported that TMA could interact with the carbonyl group in the same way as we suggested when reacting with polyamide.[57]

Reaction between DEZ and epoxy rings of SU-8: Due to the incomplete cross-linking of SU-8, it appears plausible for DEZ to directly react with epoxy groups via the ring opening reaction and form the -O-C-C ether bond, which would be in accordance with the observed increase of ether peak intensity during the PM-IRRAS measurement. A potential ring-opening reaction route is described in Scheme 2 (b): According to the epoxy-Lewis acid reaction mechanism,[58,59] which is similar to the first step of catalytic cationic polymerization of SU-8, the Zn atom can coordinate to the epoxide oxygen, and the ethyl group can be transferred to the epoxide carbon, thus enabling the breaking of C-O bond and the formation of O-Zn bond. Meanwhile, the water

molecules introduced into the polymer during the first infiltration synthesis cycle generates hydroxyl groups, and they can form zinc alkoxides after reacting with DEZ during the subsequent infiltration synthesis cycles, which can further react with uncross-linked epoxide rings, leading to more opened epoxy rings. The reaction between the DEZ and epoxy ring may be further assisted by the adduct formed between DEZ and carbonyl group of CP, similar to the TMA-catalyzed addition reaction proposed for the TMA infiltration in PMMA.[22,28] It is worth noting that compared with the effects of residual solvents, this direct reaction between DEZ and epoxy rings still seems to be a secondary factor for facilitating the ZnO infiltration synthesis in SU-8: Although both CP- and GBL-processed SU-8 samples featured the PM-IRRAS spectra showing a similar degree of the epoxy ring consumption during the infiltration synthesis, the QCM results showed that the CP-processed SU-8 had a greater mass gain than the GBL-processed counterpart. This indicates that the reaction between residual solvent molecules and DEZ played a more important role in mediating the ZnO infiltration synthesis in the SU-8.

Reaction between DEZ and ether groups of SU-8: There are two kinds of ether groups in SU-8, one originating from the SU-8 monomer and the other from the cross-linked SU-8 network resulting from the ring-opening polymerization of epoxy groups. Due to the similar chemical structures, we speculate that both of them can interact with DEZ in the same manner as described in Scheme 2 (c). We note that although the consumption of ether groups has been observed during the infiltration synthesis of Al_2O_3 in several ether-containing polymers using TMA,[22,27] no specific reaction mechanism has been proposed. We recognize that despite the low chemical reactivity of the C-O-C linkage, the two pairs of electrons on the oxygen atom do offer the ether molecule some reactivity, allowing its reaction with certain acids.[60] We suggest that DEZ can be weakly attached to the oxygen atom of C-O-C group of the SU-8 to form a metastable complex, eventually leading to the formation of -Zn-OH bond in the subsequent water cycles.

Anisotropic texturing of the SU-8 film: A recent study of ZnO infiltration in P3HT, a non-reactive semi-crystalline conducting polymer, showed that the polymer crystallinity could promote the infiltration synthesis of ZnO in the polymer matrix.[31] We find from the PM-IRRAS study that the spin-coated SU-8 had a certain anisotropic chain alignment within the film, and this might have been another factor potentially beneficial for the ZnO infiltration synthesis. Figure 5 shows the IR absorption spectra obtained by PM-IRRAS from the spin-coated SU-8 films with their thicknesses varying from 40 nm to 135 nm. There is a clear increase in the IR absorption intensities of the peaks originating from SU-8 over the whole spectral range with

increasing thickness, except that the intensity of carbonyl peak from the residual solvent CP (1735 cm^{-1}) was nearly invariant. The asymmetric thickness-dependent IR absorption intensity directly results from the fact that the orientation of the SU-8 polymer chains is *anisotropic* while that of the solvent molecules is *isotropic*. This distinction is possible owing to the unique surface selection rule of the PM-IRRAS technique that utilizes the modulated polarization of incident IR light (between p- and s-polarizations): Under the p-polarized incident IR light, the only vibrations that can interact with the incident light are those with in-plane alignment of dipole moments (i.e., molecules or polymer chains aligned in plane), while both s- and p-polarized lights interact equally when the molecular orientation is isotropic. If molecules or polymer chains are randomly oriented within the spin-coated film, the thickness change should not induce any intensity change in the PM-IRRAS spectrum because the polarization modulation effectively removes the contributions from the random (i.e., isotropic) medium, and the IR absorption signal becomes sensitive only to the molecules or polymer chains situated *at the substrate surface* with specific chain alignments.[41] The observed carbonyl peak intensity invariant with the film thickness variation represents a prototypical case for the isotropic molecular orientation. On the contrary, the observed scaling of SU-8 IR absorption intensities with the film thickness indicates that there exist anisotropic in-plane alignments of SU-8 polymer chains through the film thickness. The observation is consistent with other studies that showed a similar anisotropic SU-8 polymer texturing caused by stress conditions developed during the spin-casting process.[42] A separate experiment, wherein we manually controlled the s- and p-polarization of incident IR light (Figure S6), suggested the perpendicular (edge-on) chain alignment in the cross-linked SU-8 film (most likely in a very short range considering that the cross-linked SU-8 should be highly branched), which may help the diffusion of DEZ molecules into the polymer matrix during the initial infiltration synthesis cycle.

SU-8 chain conformation: A closer examination of PM-IRRAS data reveals the conformational changes of SU-8 polymer chains upon the ZnO infiltration, which should also assist the physical accommodation of infiltration-synthesized ZnO within the SU-8 matrix. In Figure 2 (c), the ZnO infiltration synthesis induced a variation in the IR absorption features related with the benzene moieties[35] of SU-8. Specifically, there was an increase of the absorption peak intensities at 1608 cm^{-1} and 1580 cm^{-1}, accompanied by a slight decrease in the peak intensities at 1508 cm^{-1} and 1470 cm^{-1}, after the ZnO infiltration synthesis. The two former peaks generally correspond to the in-phase ring stretching vibrations of benzene rings contained in the cross-linked SU-8, which can be either in the backbone of the SU-8 network (ortho-substituted benzene) or in the side

chain (para-substituted benzene). The latter two peaks at 1508 cm^{-1} and 1470 cm^{-1} with decreased intensities are also assigned to the para- and ortho-substituted benzene rings, respectively. Considering that the benzene rings do not participate in any chemical reaction,[45] the observed variation in the PM-IRRAS peak intensity is most likely attributed to the changes in the molecular orientation and the chemical environment, which in this case are related with the SU-8 chain conformation occurring during the ZnO infiltration synthesis and the physical inclusion of synthesized ZnO into the polymer free volume.

4. CONCLUSION

The effects of residual processing solvent molecules enabling the ZnO infiltration synthesis in the non-reactive SU-8 polymer was discovered by the systematic investigation combining the QCM, PM-IRRAS, XPS, and cross-sectional TEM experiments that respectively interrogated the mass gain, chemical, and structural characteristics of the SU-8 thin film influenced by the ZnO infiltration synthesis. From the PM-IRRAS and XPS data, we found that the infiltrating Zn precursor DEZ was reacting with the carbonyl groups of CP, the processing solvent molecules residual within the cross-linked SU-8, enabling the ZnO infiltration synthesis in the nominally non-reactive SU-8 matrix. This was clearly supported by the mass gain measured during the infiltration synthesis and the ZnO-infiltrated internal structure studied by TEM. A comparative study examining a different type of processing solvent (GBL) augmented the notion that the residual solvent molecules could influence the extent of infiltration synthesis in the non-reactive polymer matrix. Further analyses of PM-IRRAS data revealed other factors potentially beneficial to the ZnO infiltration synthesis in SU-8, including the direct reaction of DEZ with uncross-linked residual epoxy rings of SU-8, the anisotropic in-plane alignment of SU-8 polymer chains, and the chain conformation that could accommodate the physical inclusion of the infiltration-synthesized ZnO within the polymer matrix. By considering generally known reactions available to DEZ, we proposed a few potential reaction routes that enabled the reaction of DEZ with the SU-8 matrix, such as the addition reaction of DEZ with the C=O group of CP; the opening of uncross-linked epoxy rings of SU-8 by DEZ, and the weak complexation of DEZ with the ether backbone of SU-8 polymer network. We acknowledge that the future in-situ IR characterization directly investigating the DEZ reaction with the suggested chemical moieties will be valuable to examine the validities of the proposed reaction mechanisms and further advance the understanding of the fundamental processes responsible for the infiltration synthesis.

Overall, the results represent the first identification of the effect of processing solvents enabling the infiltration synthesis in polymers in general. If the discovered effect can be properly controlled (e.g., by varying the polymer thermal processing condition (temperature etc.) to adjust the amount of residual solvent in the polymer matrix; intentionally dispersing a controlled amount of reactive molecules in the polymer; or solvent annealing), our finding should be able to further expand the application of infiltration synthesis to the generation of functional organic-inorganic hybrids and inorganic nanostructures based on more diverse types of polymers.

REFERENCES

(1) Ramanathan, M.; Tseng, Y.-C.; Ariga, K.; Darling, S. B. Emerging Trends in Metal-Containing Block Copolymers: Synthesis, Self-Assembly, and Nanomanufacturing Applications. *J. Mater. Chem. C* **2013**, *1*, 2080–2091.

(2) Cummins, C.; Ghoshal, T.; Holmes, J. D.; Morris, M. A. Strategies for Inorganic Incorporation Using Neat Block Copolymer Thin Films for Etch Mask Function and Nanotechnological Application. *Adv. Mater.* **2016**, *28*, 5586–5618.

(3) Elam, J. W.; Biswas, M.; Darling, S.; Yanguas-Gil, A.; Emery, J. D.; Martinson, A. B. F.; Nealey, P. F.; Segal-Peretz, T.; Peng, Q.; Winterstein, J.; Liddle, J. A.; Tseng, Y.-C. New Insights into Sequential Infiltration Synthesis. *ECS Trans.* **2015**, *69*, 147–157.

(4) Kamcev, J.; Germack, D. S.; Nykypanchuk, D.; Grubbs, R. B.; Nam, C. Y.; Black, C. T. Chemically Enhancing Block Copolymers for Block-Selective Synthesis of Self-Assembled Metal Oxide Nanostructures. *ACS Nano* **2013**, *7*, 339–346.

(5) Lee, S.-M.; Pippel, E.; Gösele, U.; Dresbach, C.; Qin, Y.; Chandran, C. V.; Bräuniger, T.; Hause, G.; Knez, M. Greatly Increased Toughness of Infiltrated Spider Silk. *Science.* **2009**, *324*, 488–492.

(6) Yu, Y.; Li, Z.; Wang, Y.; Gong, S.; Wang, X. Sequential Infiltration Synthesis of Doped Polymer Films with Tunable Electrical Properties for Efficient Triboelectric Nanogenerator Development. *Adv. Mater.* **2015**, *27*, 4938–4944.

(7) Tseng, Y. C.; Peng, Q.; Ocola, L. E.; Elam, J. W.; Darling, S. B. Enhanced Block Copolymer Lithography Using Sequential Infiltration Synthesis. *J. Phys. Chem. C* **2011**, *115*, 17725–17729.

(8) Peng, Q.; Tseng, Y. C.; Darling, S. B.; Elam, J. W. Nanoscopic Patterned Materials with Tunable Dimensions via Atomic Layer Deposition on Block Copolymers. *Adv. Mater.* **2010**, *22*, 5129–5133.

(9) Materials, N.; Templates, B. C. A Route to Nanoscopic Materials via Sequential Infiltration Synthesis on Block Copolymer Templates. *ACS Nano* **2011**, *5*, 4600–4606.

(10) Gong, B.; Peng, Q.; Jur, J. S.; Devine, C. K.; Lee, K.; Parsons, G. N. Sequential Vapor Infiltration of Metal Oxides into Sacrificial Polyester Fibers: Shape Replication and Controlled Porosity of Microporous/mesoporous Oxide Monoliths. *Chem. Mater.* **2011**, *23*, 3476–3485.

(11) Lee, S. M.; Pippel, E.; Moutanabbir, O.; Kim, J. H.; Lee, H. J.; Knez, M. In Situ Raman Spectroscopic Study of Al-Infiltrated Spider Dragline Silk under Tensile Deformation. *ACS Appl. Mater. Interfaces* **2014**, *6*, 16827–16834.

(12) Padbury, R. P.; Jur, J. S. Systematic Study of Trimethyl Aluminum Infiltration in Polyethylene Terephthalate and Its Effect on the Mechanical Properties of Polyethylene Terephthalate Fibers. *J. Vac. Sci. Technol. A* **2015**, *33*, 01A112.

(13) Ocola, L. E.; Gosztola, D. J.; Yanguas-Gil, A.; Suh, H.-S.; Connolly, A. Photoluminescence of Sequential Infiltration Synthesized ZnO Nanostructures. *Proc. SPIE* **2016**, *9755*, 97552C.

(14) Akyildiz, H. I.; Mousa, M. B. M.; Jur, J. S. Formation of Novel Photoluminescent Hybrid Materials by Sequential Vapor Infiltration into Polyethylene Terephthalate Fiber. *J. Appl. Phys.* **2015**, *117*, 2817–2826.

(15) Akyildiz, H. I.; Stano, K. L.; Roberts, A. T.; Everitt, H. O.; Jur, J. S. Photoluminescence Mechanism and Photocatalytic Activity of Organic–Inorganic Hybrid Materials Formed by Sequential Vapor Infiltration. *Langmuir* **2016**, *32*, 4289–4296.

(16) Barry, E.; Mane, A. U.; Libera, J. A.; Elam, J. W.; Darling, S. B. Advanced Oil Sorbents Using Sequential

Infiltration Synthesis. *J. Mater. Chem. A* **2017**, *5*, 2929–2935.

(17) Yu, Y.; Wang, X. Chemical Modification of Polymer Surfaces for Advanced Triboelectric Nanogenerator Development. *Extrem. Mech. Lett.* **2016**, *9*, 514–530.

(18) Padbury, R. P.; Halbur, J. C.; Krommenhoek, P. J.; Tracy, J. B.; Jur, J. S. Thermal Stability of Gold Nanoparticles Embedded within Metal Oxide Frameworks Fabricated by Hybrid Modifications onto Sacrificial Textile Templates. *Langmuir* **2015**, *31*, 1135–1141.

(19) Berman, D.; Guha, S.; Lee, B.; Elam, J. W.; Darling, S. B.; Shevchenko, E. V. Sequential Infiltration Synthesis for the Design of Low Refractive Index Surface Coatings with Controllable Thickness. *ACS Nano* **2017**, *11*, 2521–2530.

(20) Darling, S. B. Sequential Infiltration Synthesis Lithography Enables High-Aspect Ratio Patterning of Substrates. *Adv. Coatings Surf. Technol.* **2013**, *26*, 3–4.

(21) Nam, C. Y.; Stein, A.; Kisslinger, K.; Black, C. T. Electrical and Structural Properties of ZnO Synthesized via Infiltration of Lithographically Defined Polymer Templates. *Appl. Phys. Lett.* **2015**, *107*, 203106.

(22) Biswas, M.; Libera, J. A.; Darling, S. B.; Elam, J. W. Kinetics for the Sequential Infiltration Synthesis of Alumina in Poly(methyl Methacrylate): An Infrared Spectroscopic Study. *J. Phys. Chem. C* **2015**, *119*, 14585–14592.

(23) George, S. M. Atomic Layer Deposition: An Overview. *Chem. Rev.* **2010**, *110*, 111–131.

(24) Akyildiz, H. I.; Jur, J. S. Organometallic Exposure Dependence on Organic–inorganic Hybrid Material Formation in Polyethylene Terephthalate and Polyamide 6 Polymer Fibers. *J. Vac. Sci. Technol. A* **2015**, *33*, 20604.

(25) Ishchenko, O. M.; Krishnamoorthy, S.; Valle, N.; Guillot, J.; Turek, P.; Fechete, I.; Lenoble, D. Investigating Sequential Vapor Infiltration Synthesis on Block-Copolymer-Templated Titania Nanoarrays. *J. Phys. Chem. C* **2016**, *120*, 7067–7076.

(26) Gregorczyk, K. E.; Pickup, D. F.; Sanz, M. G.; Irakulis, I. A.; Rogero, C.; Knez, M. Tuning The Tensile Strength Of Cellulose Through Vapor Phase Metallization. *Chem. Mater.* **2014**, *27*, 181–188.

(27) Gong, B.; Parsons, G. N. Quantitative in Situ Infrared Analysis of Reactions between Trimethylaluminum and Polymers during Al2O3 Atomic Layer Deposition. *J. Mater. Chem.* **2012**, *22*, 15672–15682.

(28) Dandley, E. C.; Needham, C. D.; Williams, P. S.; Brozena, A. H.; Oldham, C. J.; Parsons, G. N. Temperature-Dependent Reaction between Trimethylaluminum and Poly(methyl Methacrylate) during Sequential Vapor Infiltration: Experimental and Ab Initio Analysis. *J. Mater. Chem. C* **2014**, *2*, 9416–9424.

(29) Biswas, M.; Libera, J. A.; Darling, S. B. New Insight into the Mechanism of Sequential Infiltration Synthesis from Infrared Spectroscopy. *Chem. Mater.* **2014**, *26*, 6135–6141.

(30) Akyildiz, H. I.; Padbury, R. P.; Parsons, G. N.; Jur, J. S. Temperature and Exposure Dependence of Hybrid Organic-Inorganic Layer Formation by Sequential Vapor Infiltration into Polymer Fibers. *Langmuir* **2012**, *28*, 15697–15704.

(31) Obuchovsky, S.; Frankenstein, H.; Vinokur, J.; Hailey, A. K.; Loo, Y.-L.; Frey, G. L. The Mechanism of Metal Oxide Deposition from ALD inside Non-Reactive Polymer Matrices: Effects of Polymer Crystallinity and Temperature. *Chem. Mater.* **2016**, *28*, 2668–2676.

(32) Khan Malek, C. G. SU8 Resist for Low-Cost X-Ray Patterning of High-Resolution, High-Aspect-Ratio MEMS. *Microelectron. J.* **2002**, *33*, 101–105.

(33) Futai, N.; Gu, W.; Takayama, S. Rapid Prototyping of Microstructures with Bell-Shaped Cross-Sections and Its Application to Deformation-Based Microfluidic Valves. *Adv. Mater.* **2004**, *16*, 1320–1323.

(34) Bednorz, M.; Urbańczyk, M.; Pustelny, T.; Papis, A. P. E.; Sidor, Z.; Kamińska, E. Application of Su8 Polymer in Waveguide Interferometer Ammonia Sensor. *Mol. Quant. Acoust.* **2006**, *27*, 31–40.

(35) Klanjšek Gunde, M.; Hauptman, N.; MačEk, M.; Kunaver, M. The Influence of Hard-Baking Temperature Applied for SU8 Sensor Layer on the Sensitivity of Capacitive Chemical Sensor. *Appl. Phys. A* **2009**, *95*, 673–680.

(36) Nam, C. Y.; Stein, A.; Kisslinger, K.; Direct Fabrication of High Aspect-Ratio Metal Oxide Nanopatterns via Sequential Infiltration Synthesis in Lithographically Defined SU-8 Templates. *J. Vac. Sci. Technol. B* **2015**, *33*, 06F201.

(37) Feng, R.; Farris, R. J. Influence of Processing Conditions on the Thermal and Mechanical Properties of SU8 Negative Photoresist Coatings. *J. Micromech. Microeng.* **2003**, *13*, 80–88.

(38) Keller, S.; Blagoi, G.; Lillemose, M.; Haefliger, D.; Boisen, A. Processing of Thin SU-8 Films. *J. Micromech. Microeng.* **2008**, *18*, 125020.

(39) Rechendorff, K.; Hovgaard, M. B.; Foss, M.; Chevallier, J.; Besenbacher, F. Bovine Serum Albumin Adsorption on Nano-Rough Platinum Surfaces Studied by QCM-D. *Colloids Surf., B* **2008**, *66*, 53–59.

(40) Frey, B. L.; Corn, R. M.; Weibel, S. C. *Polarization-Modulation Approaches to Reflection-Absorption Spectroscopy*; John M. Chalmers, P. R. G., Ed.; Wiley, 2001; Vol. 2.

(41) Buffeteau, T.; Desbat, B.; Turlet, J. M. Polarization Modulation FT-IR Spectroscopy of Surfaces and Ultra-Thin Films: Experimental Procedure and Quantitative Analysis. *Appl. Spectrosc.* **1991**, *45*, 380–389.

(42) Elzein, T.; Kreim, V.; Ghorbal, A.; Bistac, S. Structural Anisotropy in Friction-Deposited Layers of Polystyrene. *J. Polym. Sci. B* **2006**, *44*, 3272–3281.

(43) J. Kestell, et al. A Stand-Alone Polarization-Modulation Instrument Optimized for the Study of Catalytic Processes at Elevated Pressures. *submitted* **2017**.

(44) Yousfi, E. B.; Fouache, J.; Lincot, D. Study of Atomic Layer Epitaxy of Zinc Oxide by in-Situ Quartz Crystal Microgravimetry. *Appl. Surf. Sci.* **2000**, *153*, 223–234.

(45) Olziersky, A.; Barquinha, P.; Vilˋ, A.; Pereira, L.; Goṇalves, G.; Fortunato, E.; Martins, R.; Morante, J. R. Insight on the SU-8 Resist as Passivation Layer for Transparent Ga2O3 - In2O3-ZnO Thin-Film Transistors. *J. Appl. Phys.* **2010**, *108*, 64505.

(46) Maruoka, K.; Murase, N.; Bureau, R.; Ooi, T.; Yamamoto, H. Lewis Acid-Promoted Selective Rearrangement of Trisubstituted Epoxides to Aldehydes or Ketones. *Tetrahedron Lett.* **1994**, *50*, 3663–3672.

(47) Uysal, I.; Severcan, F.; Evis, Z. Characterization by Fourier Transform Infrared Spectroscopy of Hydroxyapatite Co-Doped with Zinc and Fluoride. *Ceram. Int.* **2013**, *39*, 7727–7733.

(48) Russell, J. D. Infrared Spectroscopy of Ferrihydrite: Evidence for the Presence of Structural Hydroxyl Groups. *Clay Miner.* **1979**, *14*, 109–114.

(49) Yoon, B.; O'Patchen, J. L.; Seghete, D.; Cavanagh, A. S.; George, S. M. Molecular Layer Deposition of Hybrid Organic-Inorganic Polymer Films Using Diethylzinc and Ethylene Glycol. *Chem. Vap. Depos.* **2009**, *15*, 112–121.

(50) W E Klunk, D F Covey, J. A. F. Anticonvulsant Properties of Alpha, Gamma, and Alpha, Gamma-Substituted Gamma-Butyrolactones. *Mol. Pharmacol.* **1982**, *22*, 438–443.

(51) Sridhar, G.; Gunasundari, T.; Raghunathan, R. A Greener Approach for the Synthesis of 1-N-Methyl-(spiro[2.3′]oxindolespiro[3.2″]/spiro[2.3′]indan-1,3-dionespiro[2.2″])cyclopentanone-4-Aryl Pyrrolidines. *Tetrahedron Lett.* **2007**, *48*, 319–322.

(52) Nyquist, R. A. Infrared Studies of Ketones. Infrared Studies of Ketones: Parameters Affecting the Induced Carbonyl Stretching Vibration by Solute/Solvent Interaction. *Appl Spectrosc* **1990**, *44*, 433–438.

(53) Chagnes, a; Allouchi, H.; Carré, B.; Lemordant, D. Thermal Analysis of γ-butyrolactone+1 Butyl-3-Methyl-Imidazolium Ionic Liquids Mixtures. *Solid State Ionics* **2005**, *176*, 1419–1427.

(54) Jeon, S. J.; Walsh, P. J. Asymmetric Addition of Alkylzinc Reagents to Cyclic Alpha, Beta-Unsaturated Ketones and a Tandem Enantioselective Addition/diastereoselective Epoxidation with Dioxygen. *J. Am. Chem. Soc.* **2003**, *125*, 9544–9545.

(55) *Zinc Alkyls in Organic Synthesis*; Technical Bulletin; AkzoNobel: August 2008; 1–10.

(56) Evans, D. Stereoselective Organic Reactions: Catalysts for Carbonyl Addition Processes. *Science.* **1988**, *240*, 420–426.

(57) Parsons, G. N.; Spagnola, J. C.; Gong, B.; Jur, S.; Hyde, G. K. Reactions During Atomic Layer Deposition on Polymer Films and Fibers. *ECS Meeting Abstr*. **2010**, *MA010-02*, 1411.

(58) Blank, W. J.; He, Z. A.; Picci, M. Catalysis of the Epoxy-Carboxyl Reaction. *J. Coatings Technol.* **2002**, *74*, 33–41.

(59) Saeb, M. R.; Bakhshandeh, E.; Khonakdar, H. A.; Mäder, E.; Scheffler, C.; Heinrich, G. Cure Kinetics of Epoxy Nanocomposites Affected by MWCNTs Functionalization : A Review. *Sci. J.* **2013**, *2013*, 1–14.

(60) Deruiter, J. *Ethers and Thioethers*; William B. Pratt, P. T., Ed.; Elsevier Health Sciences, 2005.

(61) Nikolic, G.; Zlatkovic, S.; Cakic, M.; Cakic, S.; Lacnjevac, C.; Rajic, Z. Fast Fourier Transform IR Characterization of Epoxy GY Systems Crosslinked with Aliphatic and Cycloaliphatic EH Polyamine Adducts. *Sensors* **2010**, *10*, 684–696.

(62) Wang, X.-B.; Sun, J.; Chen, C.-M.; Sun, X.-Q.; Wang, F.; Zhang, D.-M. Thermal UV Treatment on SU-8 Polymer for Integrated Optics. *Opt. Mater. Express* **2014**, *4*, 509–517.

(63) Lobo, H.; Bonilla, J. V. Handbook of Plastics Analysis. **2003**, 285–286.

Table 1 . Summary of the IR absorption modes of SU-8 observed by PM-IRRAS

Chemical group	Wavenumber (cm^{-1})	Assignment
Epoxy rings	1250	C-O-C asymmetric stretch [61]
	830	C-O-C symmetric stretch
	915	CH_2-O-CH bend[62]
Benzene rings	1608, 1580	1st pair of para/ortho-substituted benzene
	1508, 1410	2nd pair of para-substituted benzene
	1470	2nd pair of ortho-substituted benzene
Carbonyl group	1735	C=O stretch
Methyl groups	1385, 1362	Deformation CH_3 of C-$(CH_3)_2$ [63]
Ether groups	1184	-C-C-O-C- stretch [61]
	1128	-O-C-C- stretch
	1036	-C-O-C- stretch

Table 2 Summary of deconvoluted chemical species from the XPS data obtained from the SU-8 thin films (CP-processed) before and after 1 cycle of ZnO infiltration synthesis (Figure 3).

Sample/ No. ZnO infil. cycle	Transition	Chemical species	B.E. (eV)	FWHM (eV)	Fraction
SU-8/ 0 cycle	O 1s	C-O-C	532.9	2.32	0.70
	Sb $3d_{5/2}$	Sb_2O_5	531.1	1.50	0.13
	Sb $3d_{5/2}$	Sb_2O_3	529.8	2.03	0.17
SU-8/ 1 cycle	O 1s	C-O-C	532.9	2.23	0.49
	O 1s	Zn-O-H	531.9	1.5	0.15
	Sb $3d_{5/2}$	Sb_2O_5	531.0	1.45	0.10
	Sb $3d_{5/2}$/ O1s	Sb_2O_3 (Sb $3d_{5/2}$) + Zn-O (O 1s)	529.8	2	0.19
	Sb $3d_{5/2}$	Sb	528.0	1.6	0.68
SU-8/ 0 cycle	C 1s	C-C	284.7	1.65	0.62
	C 1s	C-O	286.5	1.89	0.34
	C 1s	C=O	288.7	2.00	0.03
	C 1s	π–π* satellite	291.4	2.04	0.01
SU-8/ 1 cycle	C 1s	C-C	284.7	1.78	0.55
	C 1s	C-O	286.4	2.17	0.36
	C 1s	C=O	289.2	1.79	0.03
	C 1s	C-Zn	282.8	1.56	0.05
	C 1s	π–π* satellite	291.1	1.72	0.01

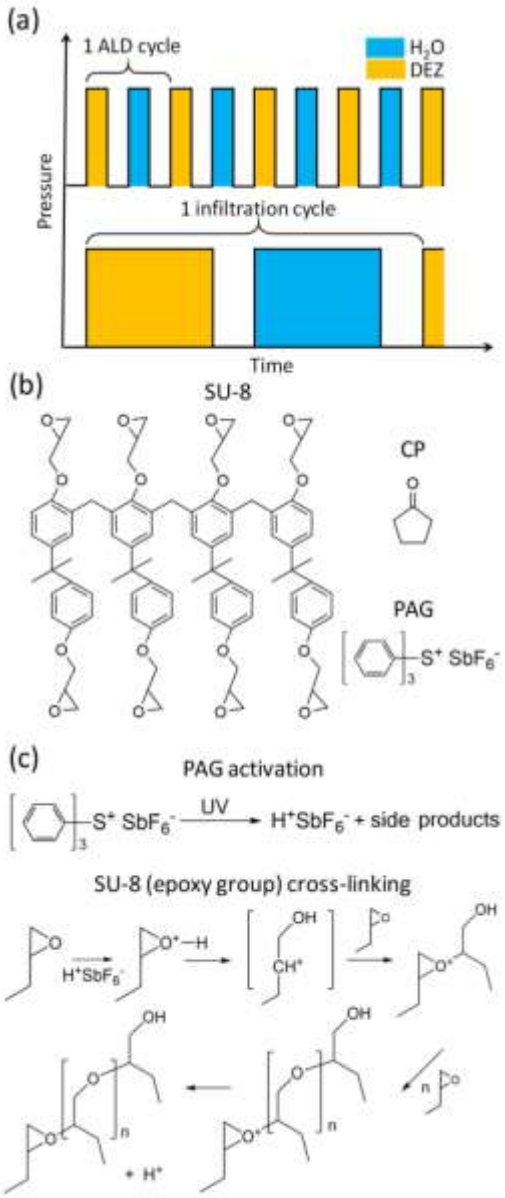

Scheme 1 Schematic description of the SIS process. Nominal molecular structures of SU-8, CP and PAG, and the reaction pathways of PAG.

(a) Schematic description of pressure vs. temperature relations during the ZnO synthesis by the normal ALD process (top) and the infiltration synthesis (bottom). Each pressure pulse represents the precursor exposure to the sample (blue: H_2O; yellow: DEZ). (b) Nominal molecular structures of SU-8 monomer, CP, and PAG ($(Ar)_3S^+SbF_6^-$). (c) Reaction pathways for the UV-activation of PAG (top) and the following cross-linking of epoxy groups of SU-8 during the post-UV-exposure thermal baking (bottom).

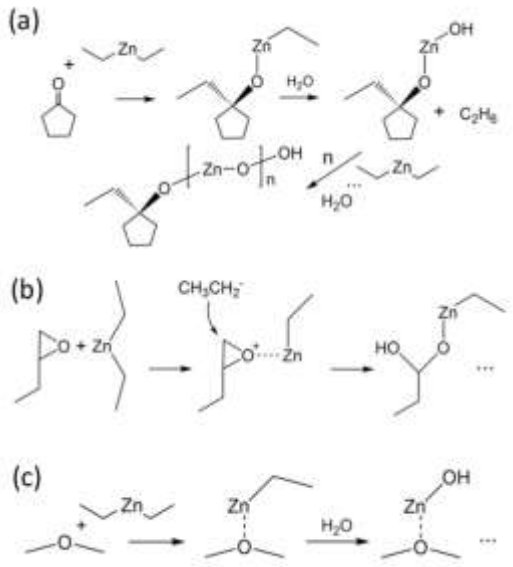

Scheme 2 Reaction pathways for the DEZ incorporation in the SU-8.

The reactions of DEZ with: (a) The carbonyl group of residual CP; (b) the uncross-linked epoxy group of SU-8; and (c) the ether bond of the cross-linked SU-8 network. The formation of ZnO by the repeating exposures of H_2O/DEZ is shown in (a) but omitted in (b) and (c).

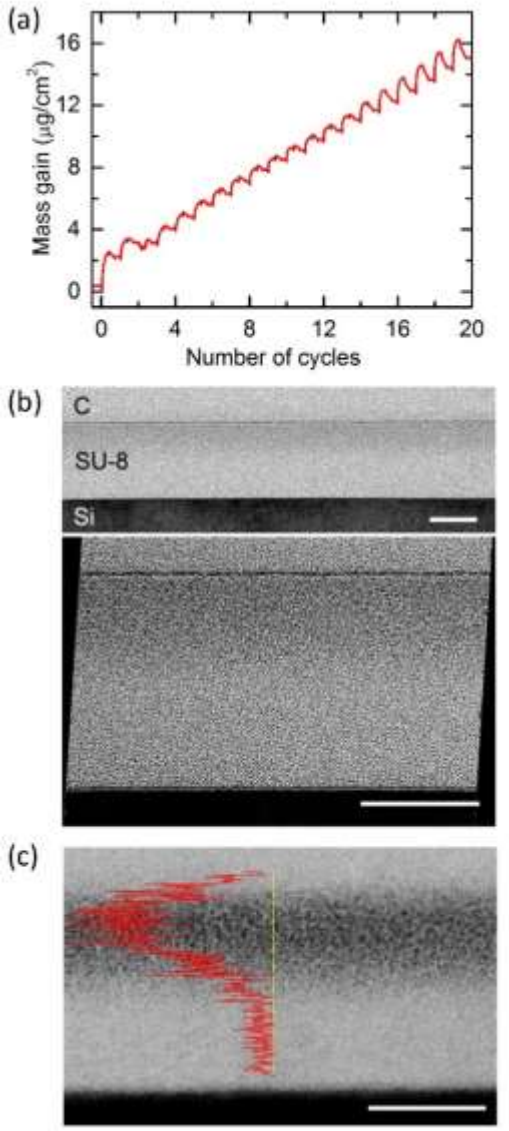

Figure 1 Mass gain data measured by QCM and TEM micrographs.

(a) Mass gain with respect to the number of ZnO infiltration synthesis cycles in the SU-8 thin film (CP-processed) measured by in-situ QCM. (b) Bright-field cross-sectional TEM micrographs of the SU-8 film after 2 cycles of ZnO infiltration synthesis (top: Low magnification; bottom: High magnification with enhanced contrast). The dark contrast on the upper portion of the film is originating from the infiltrated ZnO. C indicates the protective carbon capping layer. (c) Scanning TEM micrograph with a superimposed EDS line scan profile (red) of Zn K_α intensity along the thickness (yellow line). All scale bars denote 50 nm.

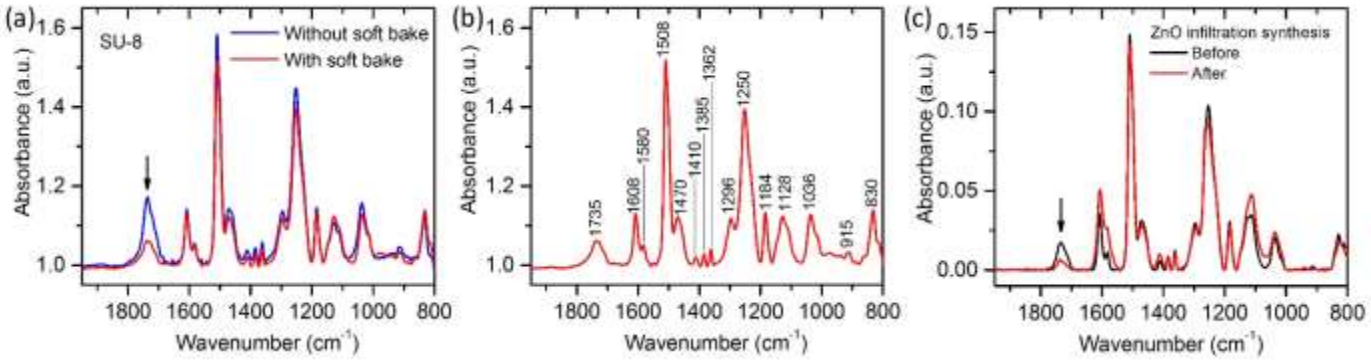

Figure 2 IR absorption spectra of SU-8 thin films (40 nm thick, CP-processed) obtained by PM-IRRAS.

(a) Comparison of SU-8 samples with (red) and without (red) soft baking, (for both, no ZnO infiltration synthesis was applied). (b) Detailed peak assignments. (c) Comparison of SU-8 samples before (black) and after (red) 4 cycles of ZnO infiltration synthesis. Arrows denote the C=O carbonyl absorption peaks.

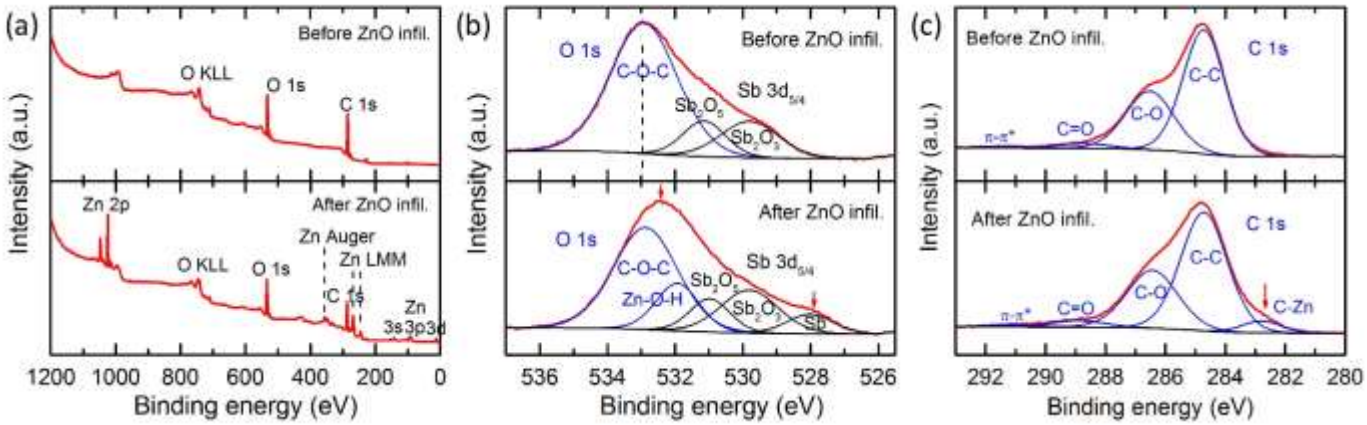

Figure 3 XPS spectra of SU-8 thin films (CP-processed) before and after 1 cycle of ZnO infiltration synthesis.

(a) Survey spectra. (b) High-resolution spectra around O 1s region. (c) High-resolution spectra around C 1s region. Red lines indicate measured spectra, and blue and black lines are deconvoluted peaks by fitting, with corresponding bonding species labeled. Red arrows denote the pronounced changes in spectra after the ZnO infiltration synthesis.

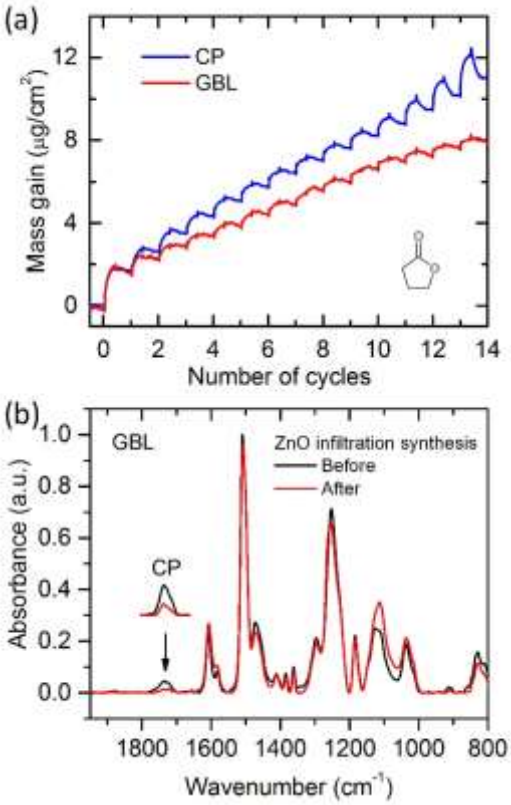

Figure 4 Mass gain characteristics and IR absorption spectra of CP and GBL processed SU-8

(a) Mass gain characteristics of SU-8 thin film processed by GBL during the ZnO infiltration synthesis (red), compared with those of CP-processed counterpart (blue). The inset shows the molecular structure of GBL. (b) IR absorption spectra of SU-8 thin films processed by GBL (40 nm thick) obtained by PM-IRRAS, before (black) and after (red) 4 cycles of ZnO infiltration synthesis. The arrow indicates the carbonyl peaks at 1735 cm^{-1}, and the inset above shows the same carbonyl peaks obtained from the CP-processed SU-8 (40 nm thick, before and after 4 cycles of ZnO infiltration synthesis) for comparison.

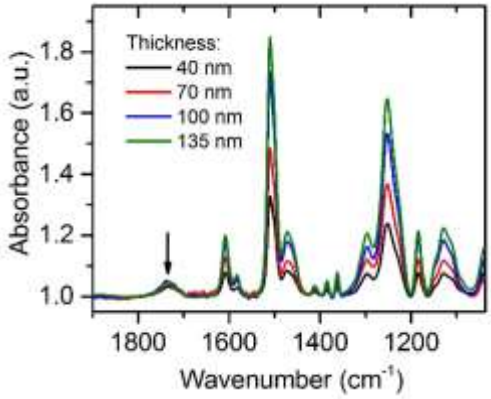

Figure 5 IR absorption spectra of SU-8 thin films (CP-processed) with varying thicknesses from 40 nm to 135 nm obtained by PM-IRRAS.

The arrow indicates the C=O carbonyl absorption peaks whose intensities are nearly constant with varying film thickness.

Supporting Information

Effects of residual solvent molecules facilitating the infiltration synthesis of ZnO in a non-reactive polymer

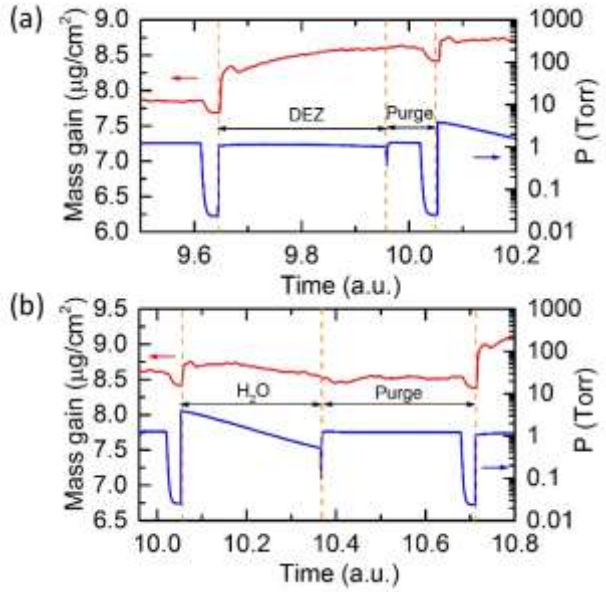

Figure S1. Representative mass gain and pressure vs. time profiles for the DEZ (a) and water (b) exposures and following purging on SU-8 thin film (CP-processed) during the ZnO infiltration synthesis cycle.

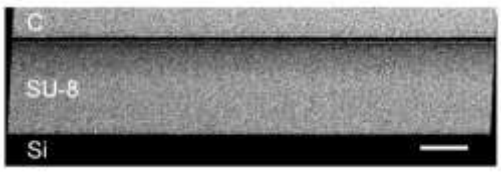

Figure S2. Bright-field, high-contrast cross-sectional TEM micrograph of the SU-8 film (CP-processed) after 10 cycles of ZnO infiltration synthesis. The dark contrast on the upper portion of the film is originating from the infiltrated ZnO. The visible ZnO infiltration depth is ~50 nm with a ~3 nm thick dense ZnO layer on top of the film. C refers to the protective carbon capping layer. The scale bar denotes 50 nm.

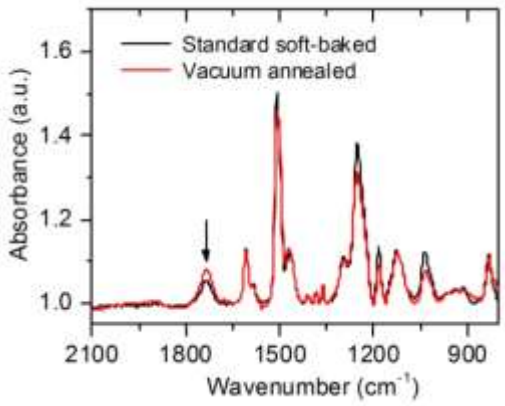

Figure S2. IR absorption spectra obtained by PM-IRRAS from the SU-8 thin films (CP-processed, 40 nm) with two different soft bake conditions: Standard soft bake (black, 65 °C-baking for 1 min followed by an additional baking at 95 °C for 3 min under an ambient air using a hot plate) vs. vacuum annealing (red, performed at 150 °C for 24 hr at ~200 mTorr pressure). The arrow indicates the C=O carbonyl absorption peaks whose intensities are nearly constant for the two soft bake conditions.

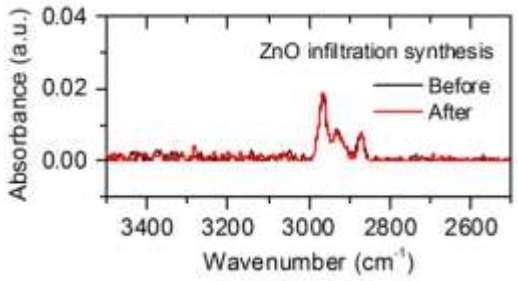

Figure S4. IR absorption spectra over 2400 cm^{-1} region obtained by PM-IRRAS from the SU-8 thin films (CP-processed, 40 nm) before (black) and after (red) 4 cycles of ZnO infiltration synthesis. There is a noticeable *absence* of the absorption peak at ~3400 cm^{-1} corresponding to the O-H stretching mode, indicating that the content of the hydroxyl group in the cross-linked SU-8 film was negligible. The three peaks at 2965 cm^{-1}, 2929 cm^{-1}, and 2871 cm^{-1} are originating from the $C\text{-}CH_3$ groups.

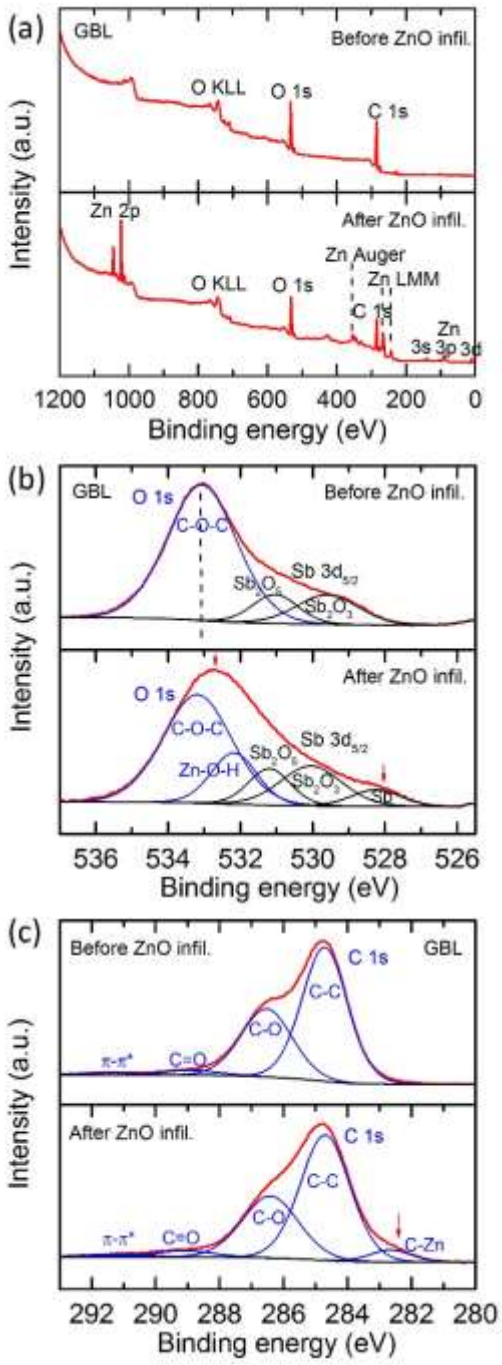

Figure S5. XPS spectra of GBL-processed SU-8 thin films before and after 1 cycle of ZnO infiltration synthesis. (a) Survey spectra. (b) High-resolution spectra around O 1s region. (c) High-resolution spectra around C 1s region. Red lines indicate measured spectra, and blue and black lines are deconvoluted peaks and backgrounds by fitting, with corresponding bonding species labeled. Red arrows denote the pronounced changes in spectra after the ZnO infiltration synthesis.

Table S1. Summary of deconvoluted chemical species from the XPS data obtained from the GBL-processed SU-8 thin films before and after 1 cycle of ZnO infiltration synthesis (Figure S2).

Sample/ No. ZnO infil. cycle	Transition	Chemical species	B.E. (eV)	FWHM (eV)	Fraction
SU-8/ 0 cycle	O 1s	C-O-C	533.1	2.26	0.75
	Sb $3d_{5/2}$	Sb_2O_5	531.0	1.48	0.11
	Sb $3d_{5/2}$	Sb_2O_3	529.6	2	0.14
SU-8/ 1 cycle	O 1s	C-O-C	533.2	2.23	0.51
	O 1s	Zn-O-H	532.2	1.49	0.16
	Sb $3d_{5/2}$	Sb_2O_5	531.2	1.38	0.11
	Sb $3d_{5/2}$/ O1s	Sb_2O_3 (Sb $3d_{5/2}$) + Zn-O (O 1s)	530.0	2.00	0.17
	Sb $3d_{5/2}$	Sb	528.3	1.60	0.05
SU-8/ 0 cycle	C 1s	C-C	284.7	1.68	0.61
	C 1s	C-O	286.6	1.87	0.35
	C 1s	C=O	288.9	2.00	0.03
	C 1s	$\pi-\pi^*$ satellite	291.4	2.00	0.01
SU-8/ 1 cycle	C 1s	C-C	284.7	1.83	0.58
	C 1s	C-O	286.4	2.06	0.32
	C 1s	C=O	289.1	2.10	0.03
	C 1s	C-Zn	282.6	1.53	0.05
	C 1s	$\pi-\pi^*$ satellite	291.2	2.34	0.02

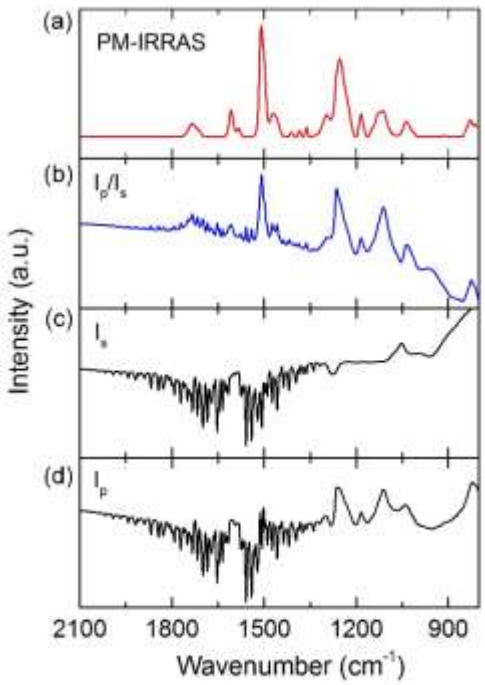

Figure S6 IR absorption spectra of the SU-8 thin film (CP-processed, 40 nm thick) without ZnO infiltration synthesis obtained under different collection methods. (a) PM-IRRAS. (b) The ratio of IR absorption measured under the p-polarized incident light (I_p) to that under the s-polarized light (I_s). (c) I_p, and (d) I_s spectra, respectively. Since the absorbance of s- and p-polarized lights are identical for an isotropic medium, the ratio should be constant if there are no preferential molecular orientations in the film. The fact that I_p/I_s spectrum clearly features positive peaks at the wavenumbers corresponding to the ether groups and phenyl rings indicates that these particular modes are interacting more with p-polarized light. Such an intensity enhancement is caused by the surface electric field of the resulting stationary wave that is normal to the metal surface [Buffeteau, T. et al., *Appl. Spectrosc.* **45**, 380 (1991)] and implies that the backbone of SU-8 polymer chains is mostly perpendicular to the substrate surface before the ZnO infiltration synthesis, which should help the incorporation of DEZ molecules into the polymer matrix during the infiltration synthesis.

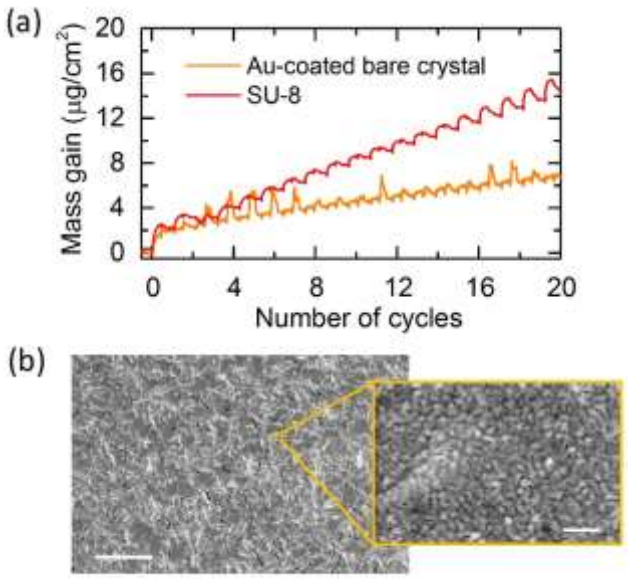

Figure S7. (a) Mass gain characteristics of SU-8 thin film (CP-processed) during the ZnO infiltration synthesis (red), compared with those of a Au-plated bare QCM crystal without SU-8 coating (orange), featuring a greater mass gain in the SU-8 due to the material infiltration into the polymer matrix. The relatively substantial mass gain on the Au-plated bare QCM crystal results from its large surface area caused by the micro/nanoscale surface roughness and pores/crevices as shown in the scanning electron micrographs in (b). Scales bars denote 8 μm (left panel) and 200 nm (right panel), respectively.